The Evolution of Communication Mechanisms in Self-Organised Ecological Aggregations

Eftimie, Raluca

Published in:
Mathematical Models and Methods in Applied Sciences

DOI:
10.1142/S0218202520400138

Publication date:
2020

Document Version
Peer reviewed version

Mathematical Models and Methods in Applied Sciences

The evolution of communication mechanisms in self-organised ecological aggregations: impact on pattern formation

R. Eftimie
Department of Mathematics, University of Dundee,
Dundee, DD1 4HN, United Kingdom
r.a.eftimie@dundee.ac.uk

Received (Day Month Year)
Revised (Day Month Year)
Communicated by (xxxxxxxxxx)

Collective behaviours in animal communities are the result of inter-individual communication. However, communication signals are not fixed; they evolve to ensure more effective interactions between the emitter and receiver of these signals. In this study we use a mathematical approach and investigate the effect of changes in communication signals (at both receiver and emitter levels) on the aggregation patterns displayed by these animal communities. We use simple linear stability analysis to study the impact that the loss/gain in signals strength has on the formation of stationary and moving animal aggregations. We then use numerical simulations to study the impact of these signal strengths on the long-term persistence of some stationary and moving aggregations. We show that a reduction in the strength of such communication signals can stop the movement of some aggregations. Moreover, for very weak signals, one can obtain a variety of standing wave patterns characterised by left-moving and right-moving waves of individuals passing through each other, with or without some individuals joining the opposite-moving group.

Keywords: 1D nonlocal kinetic model; Social aggregations; Communication between individuals.

AMS Subject Classification: 92B05, 35L40, 45K05

1. Introduction

Self-organised animal aggregations are the result of social interactions between the members of the community (e.g., attractions to some neighbours, repulsion from others). However, for these interactions to take place, animals need to communicate with each other via different signals: visual, acoustic, chemical, tactile or behavioural. These animal signals can vary spatially, temporally and qualitatively [19] in response to the environment [30]. Moreover, environmental noise can lead to the adaptation of animal communication (in terms of plasticity and evolution), especially when it comes to long-range communication signals [32]. For example, some animal species (e.g., lizards [30]) have been shown to evolve different signal strategies for effective communication in different environments with less/more noise [30].

In addition, more recent experimental research has shown that plasticity in social communication can be used by animals to facilitate their colonisation of novel habitats [31]. It should be mentioned here that while the focus of this study is on animal communication (since research in this area has been developed for more than six decades [21,27]), the ideas presented here can be further adapted to cell, bacterial, or human communication [6,20,23,25,38].

The majority of studies on animal communication usually focus on one signaller and one receiver at a time – since it is easier to understand the mechanisms of inter-individual communication in this context. However, many animals live in large communities and continuously coordinate their behaviours with their neighbours' behaviours, and thus communication occurs between many signallers and receivers at a time. Unfortunately, it is difficult to study experimentally this kind of simultaneous multi-individual communication.

Mathematical approaches could be used when experimental studies are difficult to be performed. In this context, the last few decades have seen the development of a large number of mathematical models used to investigate the biological mechanisms behind self-organised animal behaviours (from the formation of aggregations [11,12,24,34], to their collective movement [7,10,12,22,29,35]). In the majority of these models animal communication is incorporated implicitly, through the assumption that individuals can perceive their neighbours within certain spatial distances (i.e., metric interactions), and thus they adapt their behaviours to their neighbours' behaviours. However, more and more mathematical models have started to focus on topological interactions, which incorporate the assumption that an individual interacts only with a finite number of its neighbours, irrespective of their distance [3,4,5,40,44] (e.g., birds might interact with up to 6-7 of their neighbours [3], humans might interact with 5-7 of their neighbours [44]). This topological approach includes a more explicit assumption of inter-individual communication inside social aggregations. A distinct approach has been taken in [13,17,18], where the authors introduced a class of nonlocal mathematical models of hyperbolic type that can incorporate explicitly the directionality of communication signals, in addition to the spatial range over which these signals can act. The models in [13,17,18] were probably the first ones to consider the effect of changes in the directionality of such signals, on animal behaviours and aggregations. The importance of signal directionality has been supported also by some experimental studies that found, for example, that birds adjust the directionality of their calls depending on the context in which they use them: to communicate with predators (directional calls) or with conspecifics (omnidirectional calls) [43].

In this study, we consider a slight generalisation of the class of nonlocal hyperbolic models introduced in [17,18], in which we incorporate some specific parameters that measure the strength of communication signals emitted towards or received from neighbours. With the help of these parameters, we can connect all communication models introduced in [17,18], and thus we can investigate pattern formation in self-organised aggregations as communication mechanisms evolve in response to

the environment. By combining numerical simulations with linear stability analysis of steady states, we can study the impact of these parameters on both the short-term and long-term dynamics of these models, with a focus on the formation and persistence of spatial and spatio-temporal aggregation patterns.

We start in Section 2 with the description of this general class of nonlocal hyperbolic models for self-organised behaviours. In Section 3 we focus on the steady states exhibited by these models and on their stability as a result of changes in the strength of communication signals. We also investigate numerically the long-term persistence of some of the spatial and spatio-temporal patterns arising from perturbations of these steady states. We summarise and discuss the results in Section 4.

2. Model description

The following model was introduced in [17] to describe the dynamics of a population formed of right-moving (u^+) and left-moving (u^-) of individuals found inside a 1D domain, which interact with each other using different communication mechanisms:

$$\begin{cases} \frac{\partial u^+}{\partial t} + \gamma \frac{\partial u^+}{\partial x} = -\lambda^+[u^+,u^-]u^+ + \lambda^-[u^+,u^-]u^-, \\ \frac{\partial u^-}{\partial t} - \gamma \frac{\partial u^-}{\partial x} = \lambda^+[u^+,u^-]u^+ - \lambda^-[u^+,u^-]^-, \end{cases} \tag{2.1}$$

For simplicity, it is assumed the individuals in both subpopulations move at the same constant speed γ, and change their direction of movement at rates $\lambda^\pm$ upon interactions with neighbours. Since the movement of biological organisms (e.g., cells, insects, animals, humans) contains both a random and a directed component (as emphasised almost a century ago by Lotka [26], and re-iterated by many other recent studies in cell biology and ecology [2,33,36]), we assume that the turning rates $\lambda^\pm$ are described by the following equation:

$$\lambda^\pm[u^+,u^-] = \lambda_1 + \lambda_2 f\big(y_r^\pm[u^+,u^-] - y_a^\pm[u^+,u^-] + y_{al}^\pm[u^+,u^-]\big). \tag{2.2}$$

Here, λ_1 approximates the random turning of an individual, while λ_2 approximates the directed turning upon the local/nonlocal social interactions with neighbours [18]. An example of a biologically-realistic turning function f is $f(y) = 0.5 + 0.5\tanh(y-2)$ [17,18] (here $f \geq 0$, $f(0) \approx 0$, and f is increasing and bounded as a function of the social interactions y). The social interactions, namely repulsion ($y_r^\pm$), alignment ($y_{al}^\pm$) and attraction ($y_a^\pm$), occur on specific spatial ranges: repulsion acts on short ranges, alignment on medium ranges, and attraction on long ranges; see also Fig. 1. These spatial ranges (which can be distinct or overlapping) are modelled mathematically with the help of spatial kernels for repulsion (K_r), alignment (K_{al}) and attraction (K_a), as shown in Fig. 1. In this study we take the same approach as in [17] and use translated Gaussian kernels:

$$K_j(s) = \frac{1}{2\pi m_j^2}\exp(-(s-s_j)^2/(2m_j^2)), \text{ with } j = r, al, a \text{ and } m_j = s_j/8, \tag{2.3}$$

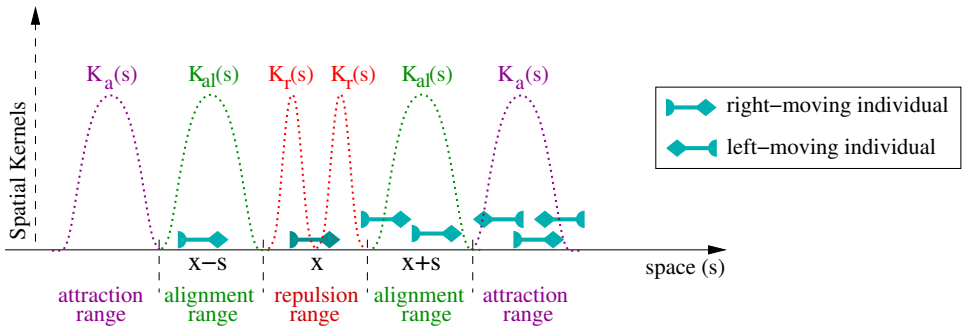

Fig. 1. Description of spatial interaction ranges on a 1D domain, for a reference individual positioned at x. Such ranges can be defined with the help of Gaussian kernels; see Eq. (2.3).

where s_j depict the middle of the spatial interaction range (s_a for attraction, s_{al} for alignment, s_r for repulsion), and m_j control the width of these ranges.

To describe these social interactions between neighbours, we focus on the inter-individual communication. In [17], the authors proposed a few communication mechanisms where individuals can perceive/emit signals from/to their neighbours in a unidirectional or omnidirectional manner. A generalisation of these mechanisms, which includes parameters for different strengths of perception/emission of signals, is shown in Fig. 2 and described by the integral terms in Table 1.

Remark 1. In [17] the authors introduced also a communication model called "M1", which was a combination of model M2 (for attraction/repulsion) and model M4 (for alignment). Since this model did not show any new results in terms of pattern formation (compared to models M2 and M4)[17], we will ignore it in this study.

Note that models M2 and M4 describe *omnidirectional perception* of signals form neighbours, while models M3 and M5 describe *directional perception* of signals coming only from ahead (with respect to the movement direction of the reference individual at x). Moreover, models M2 and M3 describe *omnidirectional emission* of signals by neighbours, while models M4 and M5 describe *directional emission* of signals by these neighbours. The connection between these different communication mechanisms is illustrated in Fig. 3.

Most of the previous studies focused on this class of models (2.1) assumed that whenever individuals perceive their neighbours positioned behind them (i.e., $p_b > 0$), they do so in a manner similar to the perception of neighbours ahead of them, i.e., $p_b = p_a = 1$ [14,17]. Those studies also assumed that neighbours emit signals in a similar manner behind and ahead of them, i.e., $e_b = e_a = 1$ [14,17]. However, these assumptions are not very biologically realistic – especially since individuals in a group could have physiological constraints that might not allow them to perceive very well signals from their neighbours behind, or might not emit signals that could be perceived by neighbours behind.

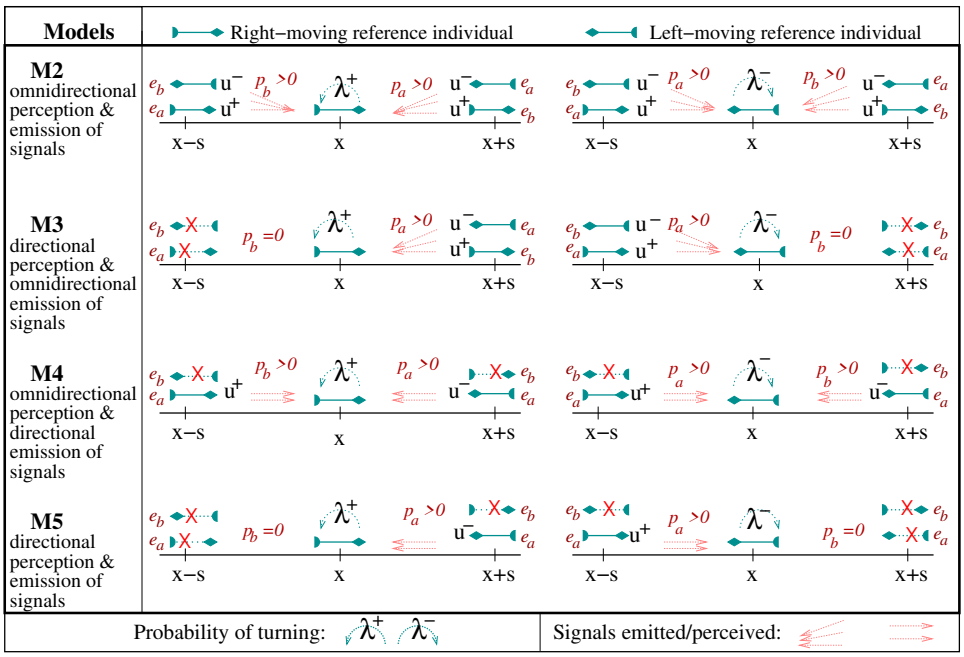

Fig. 2. Description of four possible communication mechanisms introduced in [17]: M2, M3, M4, M5. We consider a reference individual positioned at x (i.e., $u^{\pm}(x,t)$), who can perceive its neighbours positioned ahead and/or behind with respect to its moving direction. Parameters p_a and p_b describe the magnitude/strength of perception of neighbours ahead and behind, respectively. If $p_b = 0$, it means no perception of neighbours positioned behind. The red "X" mark denotes that no signals are perceived from those individuals. Parameters e_a and e_b describe the magnitude/strength of signals emitted towards the neighbours ahead and behind, respectively.

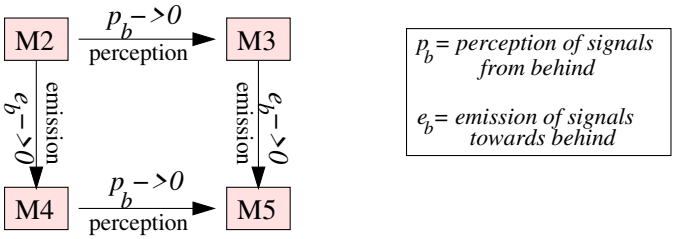

Fig. 3. Diagram describing of the connection between the models M2, M3, M4 and M5 depicted in Fig. 2 and Table 1.

In the following we will use this class of nonlocal mathematical models (2.1) to investigate the following aspects in the context of the evolution of perception and emission of signals:

- what happens, in terms of pattern formation, if $p_a > p_b > 0$ and/or

Model	Attraction ($y_a^{\pm}$), Repulsion ($y_r^{\pm}$), Alignment ($y_{al}^{\pm}$)
M2	$y_{r,a}^{\pm} = q_{r,a}\int_0^{\infty} K_{r,a}(s)\big[p_a(e_{b,a}u^+ + e_{a,b}u^-)(x \pm s,t) - p_b(e_{b,a}u^- + e_{a,b}u^+)(x \mp s,t)\big]ds,$ $y_{al}^{\pm} = q_{al}\int_0^{\infty} K_{al}(s)\big[p_a e_a u^{\mp}(x \pm s,t) + p_b e_b u^{\mp}(x \mp s,t) - p_a e_b u^{\pm}(x \pm s,t) - p_b e_a u^{\pm}(x \mp s,t)\big]ds;$
M3	$y_{r,a}^{\pm} = q_{r,a}\int_0^{\infty} K_{r,a}(s)p_a\big[e_{b,a}u^+(x \pm s,t) + e_{a,b}u^-(x \pm s,t)\big]ds,$ $y_{al}^{\pm} = q_{al}\int_0^{\infty} K_{al}(s)\big[p_a e_a u^{\mp}(x \pm s,t) - p_a e_b u^{\pm}(x \pm s,t)\big]ds;$
M4	$y_{r,a}^{\pm} = q_{r,a}\int_0^{\infty} K_{r,a}(s)\big[p_a e_a u^{\mp}(x \pm s,t) - p_b e_a u^{\pm}(x \mp s,t)\big]ds,$ $y_{al}^{\pm} = q_{al}\int_0^{\infty} K_{al}(s)\big[p_a e_a u^{\mp}(x \pm s,t) - p_b e_a u^{\pm}(x \mp s,t)\big]ds;$
M5	$y_{r,a}^{\pm} = q_{r,a}\int_0^{\infty} K_{r,a}(s)\big[p_a e_a u^{\mp}(x \pm s,t)\big]ds,$ $y_{al}^{\pm} = q_{al}\int_0^{\infty} K_{al}(s)\big[p_a e_a u^{\mp}(x \pm s,t)\big]ds.$

Table 1. Description of possible communication mechanisms introduced in [17]. Here $K_r(s)$, $K_{al}(s)$, $K_a(s)$ are the kernels describing the spatial region over which the three social interactions take place; see Fig.1. In [17] the authors used translated Gaussian kernels (2.3). Parameters q_r, q_{al} and r_a represent the magnitudes of these social interactions. Parameters p_a and p_b represent the magnitude of perception, by the reference individual at x, of its neighbours positioned ahead of it ("p_a") and behind it ("p_b"). Parameters e_a and e_b describe the magnitude of signals emitted by neighbours at $x \pm s$ towards the reference individual positioned ahead ("e_a") or behind ("e_b") of these neighbours. For a detailed description of these parameters and their values see also Table 2. Total population density is $u(x,t) = u^+(x,t) + u^-(x,t)$.

$e_a > e_b > 0$ (i.e., when we assume that there are differences in the perception/emission of signals from/towards neighbours ahead/behind a reference individual)?

- what happens, in terms of pattern formation, when $p_b \to 0$ and/or $e_b \to 0$, and thus the inter-individual communication evolves as illustrated in Fig. 3?

To address these questions, we start in Section 3.1 by discussing briefly the spatially homogeneous steady states displayed by model (2.1) and the stability of these states, as we vary $p_b, e_b \in [0,1]$. This will give us some understanding on the effects of p_b and e_b on the short-term dynamics of (2.1). Then, in Section 3.2, we investigate numerically the long-term behaviour of (2.1) by focusing on the spatio-temporal patterns that appear and/or disappear when we vary p_b and e_b.

3. Results

Throughout this study we assume that the 1D domain is finite: $x \in [0, L]$. For the purpose of the numerical simulations, we consider periodic boundary conditions

(which allow us to track moving aggregations for a long time):

$$u^+(0,t) = u^+(L,t),\ u^-(L,t) = u^-(0,t). \tag{3.1}$$

Note that arena-like domains have been used in experimental studies focused on the collective movement of insects[7].

This assumption of a finite spatial domain will have an impact on both the linear stability results in Section 3.1 (where the unstable wavenumbers will be discrete), as well as on the numerical results in Section 3.2 (where the integrals will have to be wrapped around the domain, due to the periodic boundary conditions).

The parameter values used for all results presented in this section are summarised in Table 2.

Parameter	Value	Description
L	10	Domain size
γ	0.1	Constant speed
λ_1	0.2	The random component of the turning rate
λ_2	0.9	The directed component of the turning rate
s_r	0.25	The mid point of the inter-individual repulsion range
s_{la}	0.5	The mid point of the inter-individual alignment range
s_a	1.0	The mid point of the inter-individual attraction range
m_r	$s_r/8$	Parameter controlling the width of the repulsion range
m_{al}	$s_{al}/8$	Parameter controlling the width of the alignment range
m_a	$s_a/8$	Parameter controlling the width of the attraction range
q_r	2	Strength of the repulsion interactions
q_{al}	2	Strength of the alignment interactions
q_a	2.1	Strength of the attractive interactions
p_b	$0-1$	Perception strength of neighbours positioned *behind* a reference individual
p_a	1	Perception strength of neighbours positioned *ahead* of a reference individual
e_b	$0-1$	Strength of signals emitted (by neighbours at $x \pm s$) towards a reference individual positioned *behind* them
e_a	1	Strength of signals emitted (by neighbours at $x \pm s$) toward a reference individual positioned *ahead* of them

Table 2. Description of the parameters that appear in model (2.1)-(2.2), with the nonlocal interaction terms described in Table 1. The parameters have values similar to those in [14,16,17].

3.1. *Spatially Homogeneous Steady States as* $p_b, e_b \to 0$

In the following we focus on the changes in the spatially homogeneous steady states $u^+(x,t) = u^+_*$ and $u^-(x,t) = u^-_*$, as we vary parameters p_b and e_b. These states

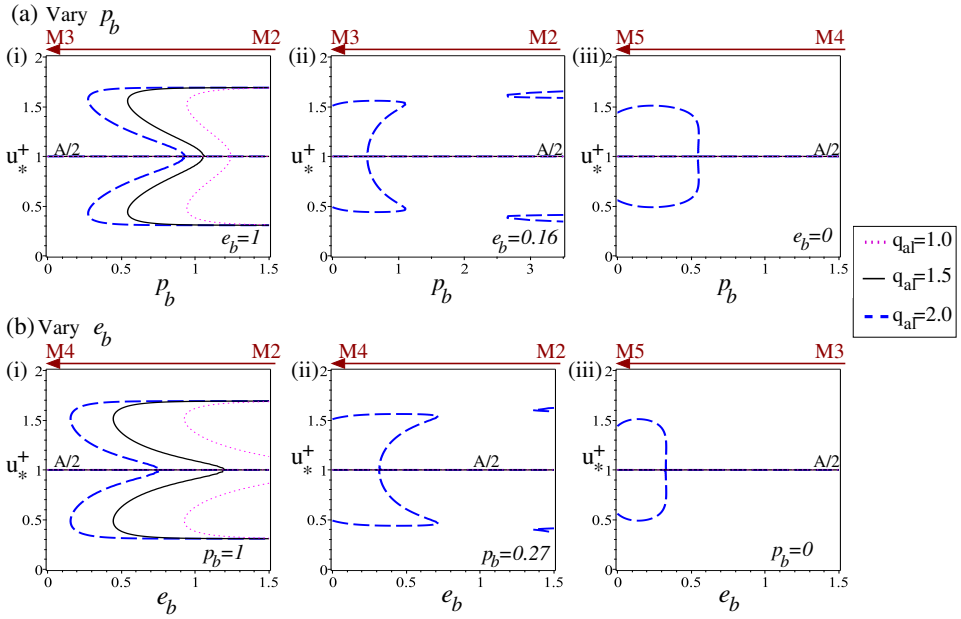

Fig. 4. Examples of spatially-homogenous steady states u^+_* exhibited by (2.1) as we fix most of all parameters and decrease: (a) $p_b = 1.5 \to p_b = 0$ (for different e_b values), and (b) $e_b = 1.5 \to e_b = 0$ (for different p_b values). To obtain these curves, we substitute $u^-_* = A - u^+_*$ into (3.2). The blue dashed curves were obtained for $q_{al} = 1$, the black continuous curves were obtained for $q_{al} = 1.5$, the red dotted curves were obtained for $q_{al} = 1.0$. Moreover, we choose $q_a = 1.1$, $q_r = 1.0$. The rest of parameter values are as in Table 2.

are characterised by individuals equally spread over the whole domain, but facing different directions (i.e., left or right). Note that system (2.1) preserves the total population density over the domain $[0, L]$, and thus $u^+_* + u^-_* = A = \frac{1}{L}\int_0[u^+(x) + u^-(x)]dx$. The most general steady state equation (obtained for $p_b \neq 0$ and $e_b \neq 0$) corresponds to model M2, and is given by:

$$\begin{aligned} 0 = -u^+_*\Big[\lambda_1 + \lambda_2 f\big((q_r - q_a)(p_a e_b u^+_* + p_a e_a u^-_* - p_b e_a u^+_* - p_b e_b u^-_*) + \\ q_{al}(p_a e_a u^-_* + p_b e_b u^-_* - p_a e_b u^+_* - p_b e_a u^+_*)\big)\Big] \\ +u^-_*\Big[\lambda_1 + \lambda_2 f\big((q_r - q_a)(p_a e_a u^+_* + p_a e_b u^-_* - p_b e_b u^+_* - p_b e_a u^-_*) + \\ q_{al}(p_a e_a u^+_* + p_b e_b u^+_* - p_a e_b u^-_* - p_b e_a u^-_*)\big)\Big]. \end{aligned} \tag{3.2}$$

We graph this equation in Fig. 4, to show the possible spatially homogeneous steady states displayed by equations (2.1) as we vary: (a) p_b and (b) e_b. Note that all models M2-M5 display the steady state with $u^+_* = u^-_* = 1$ $(= A/2)$, where half of the individuals are facing right and half are facing left. This state occurs irrespective of the q_{al} values (or other parameter values). As shown in Fig. 4, for specific alignment (q_{al}) values, it is possible to obtain another 2 or 4 steady states, characterised by

more individuals facing left than right (i.e., $u_*^+ < A/2 = 1$, $u_*^- > A/2 = 1$), or more individuals facing right than left (i.e., $u_*^+ > A/2 = 1$, $u_*^- < A/2 = 1$). These extra states exist for intermediate values of e_b and p_b. The number of these steady states is a result of the $\mathbb{O}(2)$ symmetry characterising model (2.1) [8,9].

Linear stability results. Next we focus on the steady state $u_*^+ = u_*^- = A/2$, which exists for all communication models M2-M5, and investigate its linear stability as we vary p_b and e_b. (These linear stability results will give us a basic understanding of the short-term dynamics of model (2.1) – as this analysis is valid only for short time; see also Fig. 6). To this end, we perturb the steady states as follows:

$$u^{\pm}(x,t) = u_*^{\pm} + \epsilon_{\pm} e^{\sigma t + ikx},$$

where σ describes the growth/decay of perturbations, and k is the wavenumber that can become unstable following these perturbations. Following the substitution of these expressions for $u^{\pm}(x,t)$ into the hyperbolic system (2.1), we obtain a dispersion relation that describes the connection between σ and k, for different model parameters:

$$\sigma_{1,2} = -0.5(B_1+B_2) \pm 0.5\sqrt{(B_1+B_2)^2 - 4\gamma i k(B_1-B_2) - 4\gamma^2 k^2}, \tag{3.3}$$

with

$$B_1 = \lambda_1 + \lambda_2 f_-(u_*^{\pm}) - u_*^+ \lambda_2 f'_+(u_*^{\pm}) C_{12} + u_*^- \lambda_2 f'_-(u_*^{\pm}) C_{22}, \tag{3.4a}$$

$$B_2 = \lambda_1 + \lambda_2 f_+(u_*^{\pm}) + u_*^+ \lambda_2 f'_+(u_*^{\pm}) C_{11} - u_*^- \lambda_2 f'_-(u_*^{\pm}) C_{21}, \tag{3.4b}$$

$$C_{11} = p_a e_b \big[q_r \hat{K}_r^+ - q_a \hat{K}_a^+\big] - p_b e_a \big[q_r \hat{K}_r^- - q_a \hat{K}_a^-\big] - q_{al}\big[e_b p_a \hat{K}_{al}^+ + e_a p_b \hat{K}_{al}^-\big], \tag{3.4c}$$

$$C_{12} = p_a e_a \big[q_r \hat{K}_r^+ - q_a \hat{K}_a^+\big] - p_b e_b \big[q_r \hat{K}_r^- - q_a \hat{K}_a^-\big] + q_{al}\big[e_a p_a \hat{K}_{al}^+ + e_b p_b \hat{K}_{al}^-\big], \tag{3.4d}$$

$$C_{21} = p_a e_a \big[q_r \hat{K}_r^- - q_a \hat{K}_a^-\big] - p_b e_b \big[q_r \hat{K}_r^+ - q_a \hat{K}_a^+\big] + q_{al}\big[e_a p_a \hat{K}_{al}^- + e_b p_b \hat{K}_{al}^+\big], \tag{3.4e}$$

$$C_{22} = p_a e_b \big[q_r \hat{K}_r^- - q_a \hat{K}_a^-\big] - p_b e_a \big[q_r \hat{K}_r^+ - q_a \hat{K}_a^+\big] - q_{al}\big[e_b p_a \hat{K}_{al}^- + e_a p_b \hat{K}_{al}^+\big], \tag{3.4f}$$

$$f_+(u_*^{\pm}) = f\Big((q_r - q_a)(p_a e_b u_*^+ + p_a e_a u_*^- - p_b e_a u_*^+ - p_b e_b u_*^-) + q_{al}(p_a e_a u_*^- + p_b e_b u_*^- - p_a e_b u_*^+ - p_b e_a u_*^+)\Big) \tag{3.4g}$$

$$f_-(u_*^{\pm}) = f\Big((q_r - q_a)(p_a e_a u_*^+ + p_a e_b u_*^- - p_b e_b u_*^+ - p_b e_a u_*^-) + q_{al}(p_a e_a u_*^+ + p_b e_b u_*^+ - p_a e_b u_*^- - p_b e_a u_*^-)\Big). \tag{3.4h}$$

In the above expressions we calculated the Fourier transforms of the interaction kernels

$$\hat{K}_{r,a,al}^{\pm} = \int_0^{\infty} K_{r,a,al}(s) e^{\pm iks} ds. \tag{3.5}$$

In Fig. 5 we show the dispersion relation (3.3) as we vary the perception/emission of signals, p_b and e_b. We observe that:

- for $e_b = 1$: decreasing p_b leads to a loss in patterns, since $\text{Re}(\sigma(k_j)) \to 0$, $\forall j > 0$). Moreover, when patterns form, they are the result of real bifurcations (since $\text{Re}(\sigma(k_j)) > 0$ while $\text{Im}(\sigma(k_j)) = 0$), and thus we would expect to see stationary aggregations.
- for $e_b = 0.5$: decreasing p_b leads to pattern formation via Hopf bifurcations (since $\text{Re}(\sigma(k_j)) > 0$ while $\text{Im}(\sigma(k_j)) > 0$), and thus we would expect to see travelling aggregations. The patterns have large wavenumbers, and thus we would expect to see multiple aggregations inside the domain.
- for $p_b = 1$: decreasing e_b leads to a loss of patterns with small wavenumbers (k_1, k_2, k_3) and the appearance of patterns with large wavenumbers (e.g., k_4). These new patterns arise via Hopf bifurcations.
- for $p_b = 1$: decreasing p_e leads to pattern formation via Hopf bifurcations (again, the patterns have large wavenumbers).

This linear stability analysis can describe well the short-term dynamics of model (2.1), as seen in Fig. 6. There, the dispersion relation in panel (a) predicts the initial formation of three stationary aggregations (as $\text{Re}(\sigma(k_3)) > 0$, while $\text{Im}(\sigma(k_3)) = 0$); see Fig. 6(b). These spatial aggregations are unstable, and in the long term they evolve towards a stable travelling aggregation (a rotating pulse/wave).

3.2. *Spatial and Spatio-temporal Pattern Formation*

Numerical approaches. For the numerical simulations presented in this section, we use an operator splitting approach. The advection terms are discretised using a second-order MacCormack finite difference scheme, while the reaction (turning) terms are discretised using a fourth-order Runge-Kutta scheme [37]. The integrals that appear in the social interaction terms $y^{\pm}_{r,al,a}[u^+, u^-]$ are discretised using the Simpson's method [37], and because of the periodic boundary conditions they are wrapped around the domain. The kernels $K_j(s)$ that appear inside these integrals are the translated Gaussian kernels described in the caption of Table 1.

As initial conditions for our simulations, we start again with the spatially homogeneous steady state $u^+_* = u^-_* = A/2$ (which is common for all models M2-M5, as shown in Fig. 4), and we perturb this state randomly to investigate whether aggregation patterns can form. For the purpose of this study, we consider some specific values of social interactions ($q_r = 2$, $q_{al} = 2$, $q_a = 2.1$ – see Table 2) for which the most complex communication model (M2) first exhibits three unstable *stationary aggregations*, which then evolve into a stable *travelling aggregation*; see Fig. 6. We prefer to focus on travelling aggregations since during this type of behaviour animal communication is likely impaired, with individuals easily missing information from their neighbours.

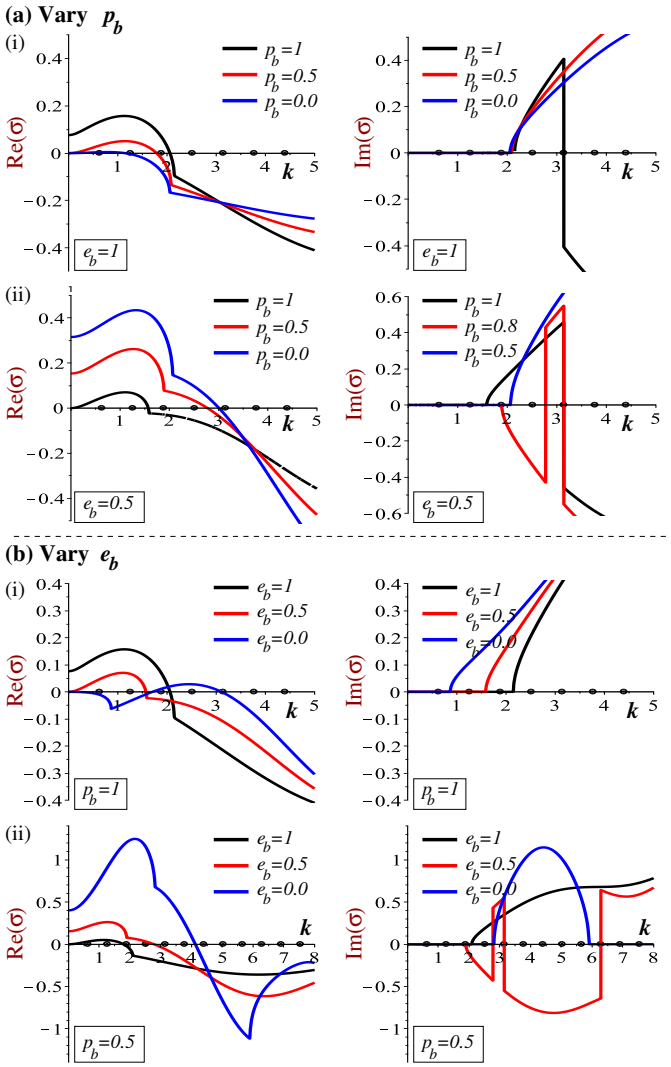

Fig. 5. Linear stability analysis for the common steady state $u_*^+ = u_*^- = 1$, as given by the real and imaginary parts of the dispersion equation (3.3) (in fact $\max(\sigma_{1,2})$), when we vary p_b and e_b. The dots on the x-axis show the discrete wavenumbers k_j. (a) We vary p_b and fix (i) $e_b = 1$ or (ii) $e_b = 0.5$. (b) We vary e_b and fix (i) $p_b = 1$ or (ii) $p_b = 0.5$. The parameter values are as in Table 2. Due to the preservation of the total density and the periodic boundary conditions on the finite domain $[0, L]$, note that $k_0 = 0$ is not an admissible wavenumber [18].

Long-term aggregation patterns. In Fig. 7 we summarise the changes in the stable spatial and spatio-temporal patterns displayed by (2.1), as we decrease p_b and e_b (while keeping all other parameters fixed as in Table 2). Here we focus on the long-term behaviour of (2.1), and record the stable spatial and spatio-temporal

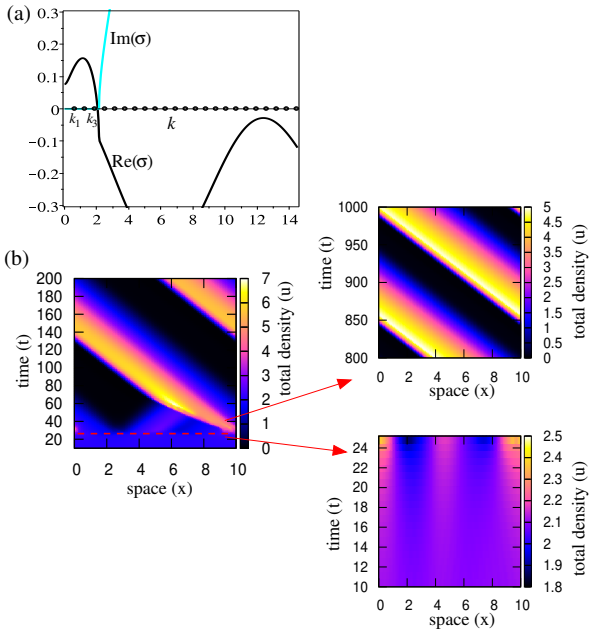

Fig. 6. (a) Linear stability of the spatially homogeneous steady state $u_*^+ = u_*^- = 1$ (as given by the dispersion relation (3.3)) for $q_a = 2.1$, $q_r = q_{al} = 2$, $p_b = p_a = e_b = e_a = 1$.The dots on the zero-axis represent the discrete wavenumbers k_j that become unstable; here we have k_3. (b) Numerical simulation of system (2.1) corresponding to the case in (a). The short-time (i.e., $t < 25$) dynamics matches the results of the linear stability analysis, with 3 stationary aggregations arising initially. The long-term (i.e., $t > 60$) dynamics shows a travelling wave.

patterns observed for $t \in [1000, 3000]$. The space-time dynamics of the various patterns summarised in Fig. 7 is shown in detail in Figs. 8 and 9.

From Fig. 7 we can deduce that for the particular parameter values investigated here (see Table 2), changes in the strength of perception/emission of communication signals (due to signal plasticity or evolution) leads to the following changes in the aggregation patterns:

- for large p_b ($p_b > 0.5$), a decrease in the e_b (which leads to M2→M4) does not have a significant impact on the travelling pulses obtained with M2 when $p_b = e_b = 1$.
- for small p_b ($p_b < 0.4$) and large e_b ($e_b > 0.2$), the aggregations become stationary. In this case, communication is dominated by the M3 model.
- for small p_b ($p_b < 0.4$), a decrease in e_b (to $e_b < 0.2$) leads to the movement of aggregations as a result of the appearance of standing waves and modulated standing waves; see also Fig. 9. These spatio-temporal patterns (which are the result of Hopf bifurcations [8,9]) are formed of waves of left-moving and right-moving densities of individuals that pass through each other, with

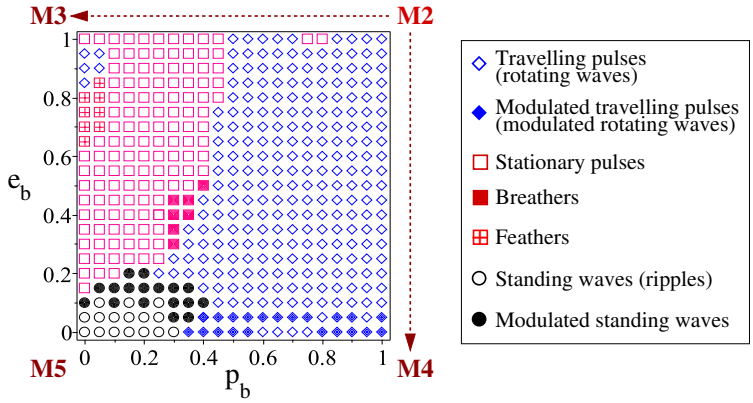

Fig. 7. Summary of the spatial and spatio-temporal patterns exhibited by model (2.1) as we vary the perception of signals from neighbours behind (p_b) and the emission of signals towards neighbours behind (e_b). Here we chose $q_a = 2.1$, $q_r = q_{al} = 2$, $p_a = e_a = 1$, for which model M2 displays a long-term travelling aggregation. The rest of parameter values are as in Table 2. For a visual description of these pattern see Figs. 8 and 9.

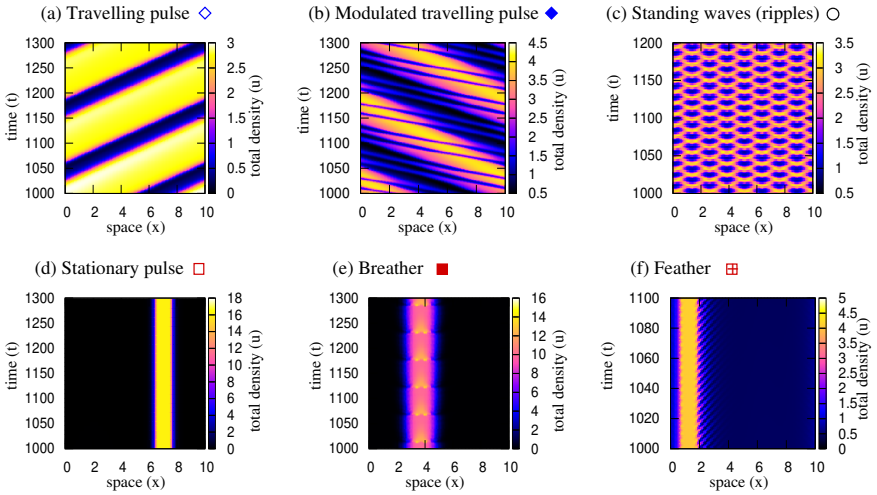

Fig. 8. Description of the spatial and spatio-temporal patterns that can be obtained with model (2.1) as we vary $p_b, e_b \in [0, 1]$, while keeping all other model parameters fixed. Here we show the total population density $u = u^+ + u^-$. The symbols next to the name of the patterns correspond to the symbols used in Fig. 7. (a) Travelling wave (pulse) for $e_b = 0.3$, $p_b = 0.75$; (b) Modulated travelling wave (pulse) for $e_b = 0.05$, $p_b = 0.55$; (c) Standing wave (ripples) for $e_b = 0.05$, $p_b = 0.25$; (d) Stationary pulse for $e_b = 1$, $p_b = 0.4$; (e) Breather for $e_b = 0.3$, $p_b = 0.3$; (f) Feather for $e_b = 0.85$, $p_b = 0.05$. All other parameter values are as in Table 2. A detailed characterisation of these patterns can be found in [13,15].

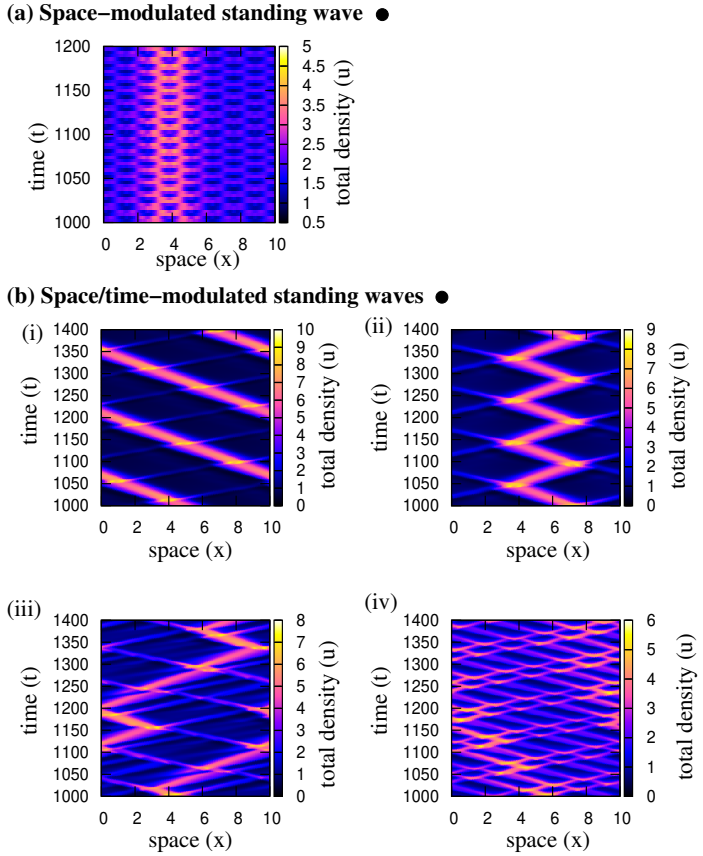

Fig. 9. Examples of space- and space/time-modulated standing waves (ripples). Here we show the total population density $u = u^+ + u^-$. The black filled circle symbol correspond to the one used in Fig. 7. All these standing waves are characterised by waves of left-moving and right-moving densities of individuals that pass through each other, with some individuals changing their original movement direction. This is in contrast with the classical standing-wave pattern (see Fig. 8(c)), where the individuals in the left-moving and right-moving waves do not change their movement direction [13]. (a) $e_b = 0.1$, $p_b = 0.1$; (b) (i) $e_b = 0.15$, $p_b = 0.35$, (ii) $e_b = 0.15$, $p_b = 0.3$, (iii) $e_b = 0.05$, $p_b = 0.3$, (iv) $e_b = 0.15$, $p_b = 0.25$.

or without individuals changing their movement directions and joining the opposite-moving group. In this case, communication is dominated by the M5 model.

- for very poor communication with neighbours behind (i.e., $p_b \in [0, 0.4]$, $e_b \in [0, 0.2]$), small perturbations in p_b and e_b can give rise to a variety of such (modulated) standing waves, as shown in Fig. 9.

Overall, the results in Fig. 7 suggest that changes in the inter-individual communication (due to environmental factors or animal physiological characteristics) might

lead to changes in the aggregation patterns they can form. However, the specific patterns shown in Fig. 7 depend on the specific parameter values used for the simulations; see Table 2. We expect that for other parameter values ($q_{r,a,al}$, $\lambda_{1,2}$ and γ) describing different types of social interactions between group members we would obtain different patterns and transitions between patterns as we vary $p_b, e_b \in [0, 1]$.

4. Discussion and Conclusions

In this study we used a class of 1D nonlocal hyperbolic models for self-organised aggregations in the presence of different communication mechanisms to investigate the impact of changes in inter-individual communication on pattern formation at community level. To this end, we focused on two parameters that control the perception of signals from neighbours behind (p_b) and the emission of signals towards neighbours behind (e_b) – relative to the movement direction of reference individuals. We investigated the impact of these two parameters on the short-term dynamics of these models (via a linear stability analysis of spatially homogeneous steady states) and long-term dynamics of these nonlocal models (via numerical simulations); see also Table 3 for a summary of the results.

Regarding the short-term dynamics of model (2.1), we observed in Fig. 5 that changes in p_b (e_b) can have opposite effects on the linear stability of steady states, depending on the magnitude of e_b (p_b). For example, for large p_b, a decrease in e_b would lead to stable steady states and no pattern formation; while for small p_b, a decrease in e_b would lead to unstable steady states and pattern formation via Hopf bifurcations. We need to emphasise here that even when the linear stability analysis suggests that the spatially homogeneous state $u_*^+ = u_*^-$ is stable, patterns can form since other steady states (with $u_*^+ \neq u_*^-$) might exist and might be unstable. Moreover, the nonlinear terms (ignored by this linear stability analysis) could push the dynamics of the model towards stable spatially-heterogeneous steady states.

Regarding the long-term dynamics of model (2.1), we observed in Fig. 7 that for some specific parameter values that lead to travelling aggregations when communication was perfect (model M2), a medium reduction in communication (M2→M3) lead to stationary aggregations. A drastic reduction in communication (M2→M5) can lead to a different type of moving aggregation, i.e., a standing wave, where left-moving and right-moving waves of individuals pass through each other. In this case, perturbation in the p_b and e_b parameters, which already have small values, has shown to lead to a large variety of spatial and spatio-temporal modulated standing waves, with some individuals more likely to turn around and join the opposite-moving wave (Fig. 9).

It is possible that, for different parameter values, we would obtain different types of patterns and transitions between patterns as we vary p_b and e_b. However, it was not the purpose of this study to investigate all these different cases. Rather, we wanted to illustrate the possible impact of changes in inter-individual communication (as as result of individuals in a group losing/gaining the ability to perceive/emit

Parameters	**Communic.**	**The effects of changes in communication on the formation/persistence of aggregations**
$p_b \approx 1$, $e_b \to 0$	M2→M4	Stationary aggregations more and more difficult to appear, but moving aggregations easier to appear Moving aggregations can persist
$p_b \to 0$, $e_b \approx 1$	M2→M3	Stationary aggregations difficult to appear Moving aggregations eventually stop moving
$p_b \to 0$, $e_b \ll 1$	M4→M5	Moving aggregations easier to appear Moving aggregations can persist, but change movement type
$p_b \ll 1$, $e_b \to 0$	M3→M5	Stationary and moving aggregations easier to appear Persistent stationary aggregations can start moving

Table 3. Summary of the analytical and numerical results obtained in this paper, as we varied two communication parameters: p_e (i.e. perception of signals from behind) and e_b (emission of signals towards behind). Changes in these two parameters lead to transitions between different communication models.

signals) on the aggregations formed by these communities of individuals.

In this study we assumed an isotropic domain, i.e., individuals have the same probability of communicating with neighbours from one side of the domain ($x \to L$) and the other side of the domain ($x \to 0$). (But they perceive differently their neighbours ahead/behind them relative to their movement direction.) For this reason, the system preserves its $\mathbb{O}(2)$ symmetry [9]. The model could be further generalised by taking the same approach as in Eftimie [16] and considering an anisotropic domain that could describe, for example, wind blowing from one specific direction (thus reducing all acoustic communication signals coming from the opposite direction).

Finally, we need to emphasise that while this study focused on animal communication, it can be generalised to communication in context of various biological aggregations: from cell-cell communication in the context of disease (e.g., cancer) and development [6,20,38,39], to bacterial communication [23,42], and to the more complex human communication [25,28,41]. However, the directionality of communication signals still needs to be clarified in the context of modelling cellular, bacterial and even human aggregations (as the current literature does not always account for the signals from the back; see the recent survey in [1].)

References

1. G. Albi, N. Bellomo, L. Fermo, S.-Y. Ha, J. Kim, L. Pareschi, D. Poyato and J. Soler, Vehicular traffic, crowds, and swarms: From kinetic theory and multiscale methods to applications and research perspectives, *Math. Models Methods Appl. Sci.* **29** (2019) 1901–2005.
2. P. Armsworth and J. Roughgarden, The impact of directed versus random movement on population dynamics and biodiversity patterns, *The American Naturalist* **165** (2005) 449–465.
3. M. Ballerini, N. Cabibbo, R. Candelier, A. Cavagna, E. Cisbani, I. Giardina, V. Lecomte, A. Orlandi, G. Parisi, A. Procaccini, M. Viale and V. Zdravkovic, Interaction ruling animal collective behaviour depends on topological rather than metric distance: Evidence from a field study, *Proc. Natl. Acad. Sci.* **105** (2008) 1232–1237.
4. N. Bellomo and F. Brezzi, Mathematical models of self-propelled particles, *Math. Models Methods Appl. Sci.* **27** (2017) 997–1004.
5. A. Blanchet and P. Degond, Kinetic models for topological nearest-neighbour interaction, *J. Stat. Phys.* **169** (2017) 929–950.
6. B. Brücher and I. Jamall, Cell-cell communication in the tumour microenvironment, carcinogenesis, and anticancer treatment, *Cell Physiol. Biochem.* **34** (2014) 213–243.
7. J. Buhl, D. Sumpter, I. Couzin, J. Hale, E. Despland, E. Miller and S. Simpson, From disorder to order in marching locusts, *Science* **312** (2006) 1402–1406.
8. P.-L. Buono and R. Eftimie, Analysis of Hopf/Hopf bifurcation in nonlocal hyperbolic models for self-organised aggregations, *Math. Models Methods Appl. Sci.* **24** (2014) 327–357.
9. P.-L. Buono and R. Eftimie, Codimension-2 bifurcations in animal aggregation model with symmetry, *SIAM J. Appl. Dyn. Syst.* **13** (2014) 1542–1582.
10. I. Couzin, Collective animal migration, *Current Biology* **28** (2018) R976–R980.
11. I. Couzin, J. Krause, R. James, G. Ruxton and N. Franks, Collective memory and spatial sorting in animal groups, *J. Theor. Biol.* **218** (2002) 1–11.
12. I. D. Couzin and J. Krause, Self-organization and collective behavior in vertebrates, in *Advances in the Study of Behaviour. Vol 32*, eds. P. Slater, J. Rosenblatt, C. Snowdon and T. Roper (Elsevier, 2003), pp. 1–76.
13. R. Eftimie, Hyperbolic and kinetic models for self-organised biological aggregations and movement: a brief review, *J. Math. Biol.* **65** (2012) 35–75.
14. R. Eftimie, Simultaneous use of different communication mechanisms leads to spatial sorting and unexpected collective behaviours in animal groups, *J. Theor. Biol.* **337** (2013) 42–53.
15. R. Eftimie, *Hyperbolic and kinetic models for self-organised biological aggregations* (Springer, Switzerland, 2018).
16. R. Eftimie, The impact of environmental noise on animal communication: pattern formation in a class of hyperbolic models for self-organised animal aggregations, *Biomath* **7** (2018) 1807217, (http://dx.doi.org/10.11145/j.biomath.2018.07.217).
17. R. Eftimie, G. de Vries and M. A. Lewis, Complex spatial group patterns result from different animal communication mechanisms, *Proc. Natl. Acad. Sci.* **104** (2007) 6974–6979.
18. R. Eftimie, G. de Vries, M. A. Lewis and F. Lutscher, Modelling group formation and activity patterns in self-organising collectives of individuals, *Bull. Math. Biol.* **69** (2007) 1537–1566.
19. C. Eliason, How do complex animal signals evolve?, *PLoS Biol.* **16** (2018) e3000093.
20. D. Ellison, A. Mugler, M. Brennan, S. Lee, R. Huebner, E. Shamir, L. Woo, J. Kim, P. Amar, I. Nemenman, A. Ewald and A. Levchenko, Cell–cell communication en-

hances the capacity of cell ensembles to sense shallow gradients during morphogenesis, *Proc. Natl. Acad. Sci.* **113** (2016) E679–E688.
21. H. Frings, Animal communication, *Am. J. Psychiatry* **118** (1962) 872–880.
22. I. Giardina, Collective behaviour in animal groups: theoretical models and empirical studies, *HFSP J.* **2** (2008) 205–219.
23. E. Greenberg, Bacterial communication and group behaviour, *J. Clin. Invest.* **112** (2003) 1288–1290.
24. D. Grünbaum and A. Okubo, Modelling social animal aggregations, in *Frontiers in Mathematical Biology. Lecture Notes in Biomathematics*, ed. S. Levin (Springer, Berlin, Heidelberg, 1994), volume 100, pp. 296–325.
25. A. King, C. Narraway, L. Hodgson, A. Weatherill, V. Sommer and S. Sumner, Performance of human groups in social foraging: the role of communication in consensus decision making, *Biol. Lett.* **7** (2011) 237–240.
26. A. Lotka, *Elements of Physical Biology* (Williams & Wilkins, Baltimore, MD, 1925).
27. P. Marler, The logical analysis of animal communication, *J. Theor. Biol.* **1** (1961) 295–317.
28. A. Morales, V. Vavilala, R. Benito and Y. Bar-Yam, Global patterns of synchronisation in human communications, *J. R. Soc. Interface* **14** (2017) 20161048.
29. A. Okubo, D. Grünbaum and L. Edelstein-Keshet, The dynamics of animal grouping, in *Diffusion and Ecological Problems: Modern perspectives. Interdisciplinary Applied Mathematics, vol 14* (Springer, New York, 2001), pp. 197–237.
30. T. Ord, G. Charles and R. Hofer, The evolution of alternative adaptive strategies for effective communication in noisy environments, *Am. Nat.* **177** (2011) 54–64.
31. T. Ord, G. Charles, M. palmer and J. Stamps, Plasticity in social communication and its implications for the colonisation of novel habitats, *Behavioral Ecology* **27** (2016) 341–351.
32. T. Ord, J. Stamps and J. Losos, Adaptation and plasticity of animal communication in fluctuating environments, *Evolution* **64** (2010) 3134–3148.
33. Y. Papastamatiou, D. Cartamil, C. Lowe, C. Meyer, B. Wtherbee and K. Holland, Scales of orientation, directed walks and movement path structure in sharks, *J. Animal Ecology* **80** (2011) 864–874.
34. J. Parrish, Complexity, pattern and evolutionary trade-off in animal aggregation, *Science* **284** (1999) 101.
35. J. Parrish, S. Viscido and D. Grünbaum, Self-organised fish schools: an examination of emergent properties, *Biol. Bull.* **202** (2002) 296–305.
36. R. Petrie, A. Doyle and K. Yamada, Random versus directionally persistent cell migration, *Nat Rev Mol Cell Biol* **10** (2009) 538–549.
37. W. Press, S. Teukolsky, W. Vetterling and B. Flannery, *Numerical Recipes: The Art of Scientific Computing* (Cambridge University Press, 2007).
38. W.-J. Rappel, Cell-cell communication during collective migration, *Proc. Natl. Acad. Sci.* **113** (2016) 1471–1473.
39. S. Schwager, P. Taufalele and C. Reinhart-King, Cell-cell mechanical communication in cancer, *Cellular and Molecular Bioengineering* **12** (2009) 1–14.
40. Y. Shang and R. Bouffanais, Influence of the number of topologically interacting neighbours on swarm dynamics, *Scientific Reports* **4** (2014) 4184.
41. S. Sumner and A. King, Actions speak louder than words in social foraging human groups, *Commun. Integr. Biol.* **4** (2011) 755–757.
42. C. Waters and B. Bassler, Quorum sensing: cell-to-cell communication in bacteria, *Annu. Rev. Cell Dev. Biol.* **21** (2005) 319–346.
43. J. Yorzinski and G. Patricelli, Birds adjust acoustic directionality to beam their an-

tipredator calls to predators and conspecifics, *Proc. R. Soc. B.* **277** (2010) 923–932.
44. Y. Yuan, X. Chen, Q. Sun and T. Huang, Analysis of topological relationships and network properties in the interactions of human beings, *PLoS ONE* **12** (2017) e0183686.